Evaluating the Early Impacts of Overcharge on a Lithium-ion Battery Cell Using the Battery Cycler Microcalorimeter Solution

Keywords: Battery, overcharging, battery safety, Battery Cycle Microcalorimeter Solution, in-operando, non-destructive, battery calorimetry, electrochemical calorimetry

MC179

ABSTRACT

Lithium plating and dendrite formation is an issue that degrades the safety, stability, and efficiency of lithium-ion and lithium metal cell chemistries. The lithium plating process can be complex but is typically an electrochemical process followed by a series of spontaneous chemical reactions. A technique that is well equipped to study electrochemically coupled chemical reactions is in-operando isothermal microcalorimetry using the Battery Cycler Microcalorimeter Solution. In this study, two identical coin cells were prepared and treated to different cycling protocols. One cell was overcharged by 50 mV and showed strong evidence for lithium plating and an internal short circuit, while the other was kept within the standard voltage window and showed no abnormal behavior. A comparison between the thermogram profiles, parasitic heat, coulombic efficiency, and voltage drop between cycles is performed for both cells. The electrochemical data showed no characteristic differences until the internal short occurred, but the heat flow displayed significant levels of instability and side reactions from the onset of overcharging. This type of non-destructive safety testing will yield unique insights into the fundamental mechanisms of cell failure and benefit early phase optimization of lithium-ion and lithium metal battery chemistries.

INTRODUCTION

Safety-related testing for lithium-ion batteries is typically destructive in nature, especially when using calorimetric techniques. Thermogravimetric analysis (TGA) and differential scanning calorimetry (DSC) are used to characterize the thermal stability profile of individual materials, or combinations of battery materials [1-3]. At the cell and module level, accelerating rate calorimetry (ARC) is often used to measure the onset of self-heating and the energy of thermal runaway [4]. When failure is initiated by heat or mechanical damage, ARC is useful for understanding what extreme conditions will cause a thermal runaway. However, when cell failure results from small changes to the internal chemistry over time, ARC does not possess the sensitivity to provide useful information about why or how the cell failed. Isothermal microcalorimetry is a higher sensitivity technique that enables studying change in the chemistry prior to what is typically considered to be the onset of cell failure and thermal runaway [5-7].

Lithium metal plating and dendrite formation is a common cause of cell failure and thermal runaway events in all lithium-ion and lithium-metal secondary cell chemistries [4, 8-10]. Lithium-ion reduction to lithium metal, shown in Equation (1), can occur whenever the intercalation of Li^+ is kinetically limited at the anode, either systemically or locally.

$$Li^+ + e^- \rightleftharpoons Li_{(S)} \qquad -3.04 \text{ V vs SHE} \qquad (1)$$

This side reaction is more commonly observed at low temperatures, during fast charge, or when the cell is overcharged [8, 11]. While the structure of lithium metal deposits can take many forms, they often grow into branch-like dendritic structures that eventually lead to an internal short circuit. These structures can also crack and generally destabilize the solid-electrolyte interface (SEI) layer, increasing the rate of interfacial parasitic reactions.

Lithium intercalation into graphite will typically take place between 0.25 V and 0.01 V vs Li/Li^+, very close to the onset of lithium plating [10]. In the absence of a reference electrode, only the relative potential difference between the anode and cathode is measured (the cell voltage), making it very difficult to differentiate these two reactions electrochemically. Electrochemical microcalorimetry, on the other hand, is well suited for this type of measurement. After lithium metal deposits on the anode, there is a spontaneous chemical reaction between the electrolyte and the metallic lithium [12]. This is a multi-step electrochemical-chemical reaction that will exhibit distinct heat flow behavior compared to a typical lithium intercalation process. Downie *et al*. published a method in 2013 using *in-situ* electrochemical microcalorimetry to study lithium plating on graphite electrodes [7]. Since this study was performed, improvements were made to the sample fixtures that were designed to increase the sensitivity and decrease the time constant of the in-operando heat flow measurement [6]. This newer system, the Battery Cycler Microcalorimeter Solution (BCMS), will be used to study lithium metal plating and internal short circuits initiated by overcharging an NMC/graphite coin cell.

METHODS

Preparation of Coin Cells

Coin cell casing, wave springs, and spacers were purchased from MTI Corporation. A premixed electrolyte composed of 1:1:1 Ethyl Carbonate (EC), Dimethyl Carbonate (DMC), and Diethyl Carbonate (DEC) in 1.0 M Lithium Hexafluorophosphate was purchased from Sigma-Aldrich. Precast and calendared lithium nickel-manganese-cobalt (NMC) 5:2:3 and graphite electrode sheets (MTI Corporation) were cut into appropriately sized disks inside an N_2 filled glovebox (<0.01 ppm H_2O). The coin cell components and relevant loadings are shown in Table 1.

Table 1. Coin Cell Composition

Cell Component	Composition	Loading
Cathode	NMC 5:2:3	12.1 mg/cm^2
Anode	Graphite	7.78 mg / cm^2
Electrolyte	1 .0 M $LiPF_6$ in 1:1:1 EC:DMC:DEC	~80 mg
Separator	Celgard™ Q165H2 Separator	2 layers

Cells were assembled in a glovebox using the configuration shown in Figure 1 and crimped using a hydraulic crimper (MTI Corporation). Once assembled, all cells were removed from the glovebox, rinsed of excess electrolyte using isopropyl alcohol, and allowed to rest for 12 hours before formation to facilitate more uniform wetting of the electrode stack. These cells had a typical capacity of 3.10 to 3.20 mAh.

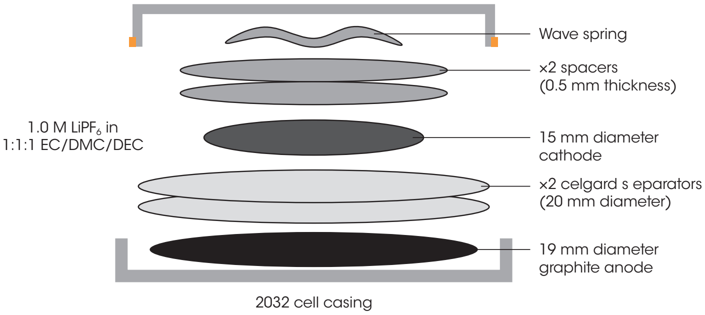

Figure 1. Coin cell configuration

Electrochemical Microcalorimetry

Testing was performed using the TA Instruments™ Battery Cycler Microcalorimeter Solution. The TAM IV Thermostat was set to 25 °C and allowed to stabilize before calibration. A microcalorimeter with twin sample and reference positions was used to measure the heat flow. The gain calibration was performed with a coin cell shaped calibration heater, containing a 1000 Ohm high precision resistor. The calibration heater was loaded in the sample chamber and an identical heater was placed in the reference and allowed to thermally equilibrate inside the microcalorimeter. A VSP-300 Potentiostat from BioLogic was used to apply current to the heater, releasing a heat pulse of known intensity. The gain and baseline offset were calculated to be 1.0074 W/W and 79.1887 nW, respectively.

After calibration, a coin cell was loaded into the sample chamber and a dry cell was loaded into the reference chamber. The dry cell had an identical configuration as the cell in the sample chamber, but with no electrolyte added, making it inert with a similar mass and heat capacity. After thermal equilibration, the cell underwent a three-stage cycling method. This method, shown in Figure 2, consists of a formation cycle, ten narrow cycles, and three full cycles. As a general precaution, this cycling method was first performed on the benchtop with a different set of cells to ensure that no electrolyte leakage, cell deformation, or thermal runaway events would occur.

Formation

- Charge with 100 µA until 3.0 V
- Rest 30 minutes
- Charge with 300 µA until 4.2 V
- Rest 1 hour
- Discharge 300 µA until 3.0 V
- Rest 1 hour

Narrow Cycles (repeat 10x)

- Charge with 300 µA until 4.2 V or 4.25 V
- Rest 1 hour
- Discharge 300 µA until 4.0 V
- Rest 1 hour

Full Cycles (repeat 3x)

- Charge with 630 µA until 4.2 V
- Rest 1 hour
- Discharge 630 µA until 3.0 V
- Rest 1 hour

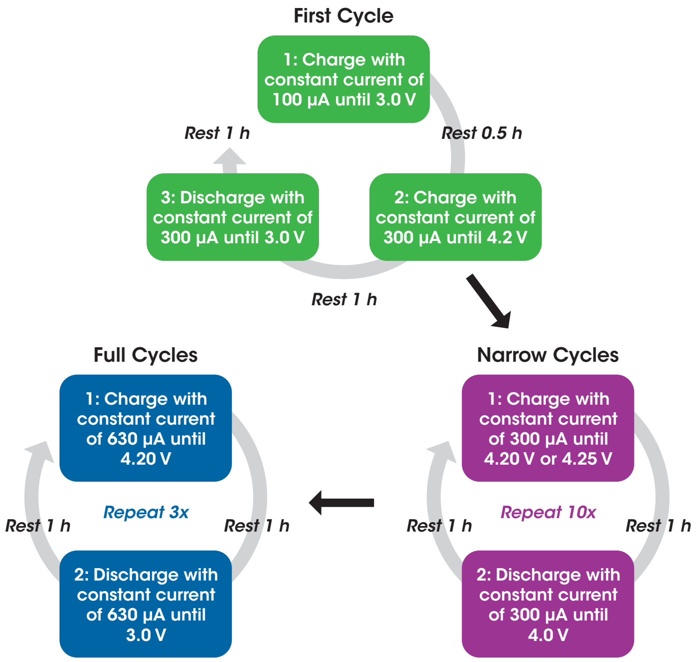

Figure 2. Cycling profile used for this experiment

Two identical coin cells were prepared using the above method, herein referred to as Cell 1 and Cell 2. Both underwent the cycling profile described in Figure 2, with Cell 1 being charged to 4.20 V during the narrow cycle phase, and Cell 2 being charged to 4.25 V. The cycling method, general composition, and handling of the cells were identical apart from this. The effects of this slight overcharging will be examined using electrochemical microcalorimetry. The behavior observed in this study is not guaranteed to occur in every cell, but the rate of side reactions will increase during overcharge, increasing the probability of a similar event.

RESULTS AND DISCUSSION

A thermogram comparing Cells 1 and 2 is shown in Figure 3. Both cells show an elevated heat flow during the first cycle due to the formation of the SEI layer. Cell 1, shown in Figure 3A, has a repeatable thermogram profile that is consistent with normal behavior. Figure 3B shows the results for Cell 2, which was overcharged by 50 mV during the narrow cycle phase. Cell 2 experienced a steady heat flow increase after day 4, roughly doubling in magnitude over one charge cycle. At this point, heat is being generated at a faster rate than can be dissipated from the cell, leading to a buildup of accumulated heat. This behavior is most likely caused by the growth of lithium dendrites leading to an internal short circuit. The internal micro-short will increase the heat generation rate as the cell continuously discharges through the internal dendrite structures. Continued cycling will amplify this process, making thermal runaway a likely outcome.

To further explore the mechanism behind the thermal behavior seen in Cell 2, portions of the thermogram are examined in greater detail. A close comparison of the entire narrow cycle phase for both cells is shown in Figure 4. Cell 1 (Figure 4A) has a repeatable profile between cycles, and the magnitude of the heat flow diminishes each cycle. This is consistent with the formation of a passivation layer, which is expected as the SEI becomes more developed. The rate of SEI growth reduces each cycle and the heat flow contribution from these reactions lessens, leading to a reduction in the total heat flow. Conversely, Figure 4B shows that Cell 2 did not experience this consistent reduction in heat flow between cycles. Instead, the heat flow is trending higher in magnitude each cycle. The exothermic events are escalating in both intensity and frequency, reflecting an increased occurrence of Li metal plating and instability for the electrode-electrolyte interface.

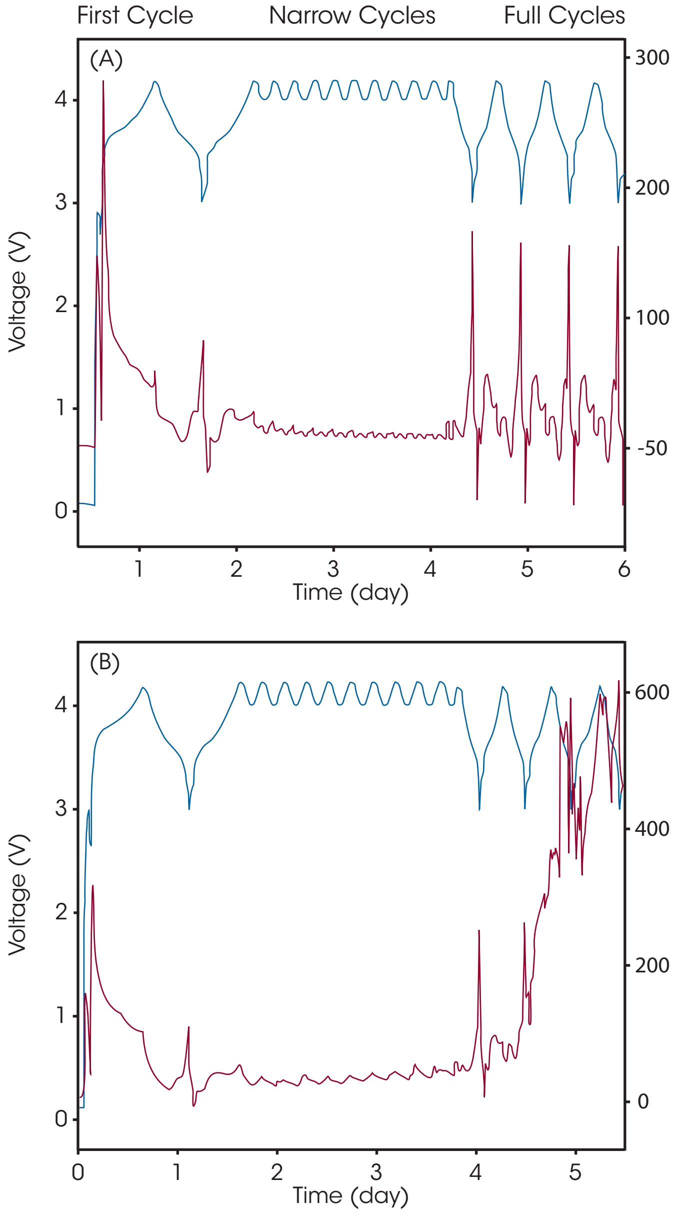

Figure 3. Comparison of thermograms for (A) Cell 1, which used an upper voltage limit of 4.2 V and (B) Cell 2, which was overcharged by 50 mV (4.25 V upper limit) during the narrow cycle phase. The blue lines are the cell voltage and the red lines are the corresponding heat flow.

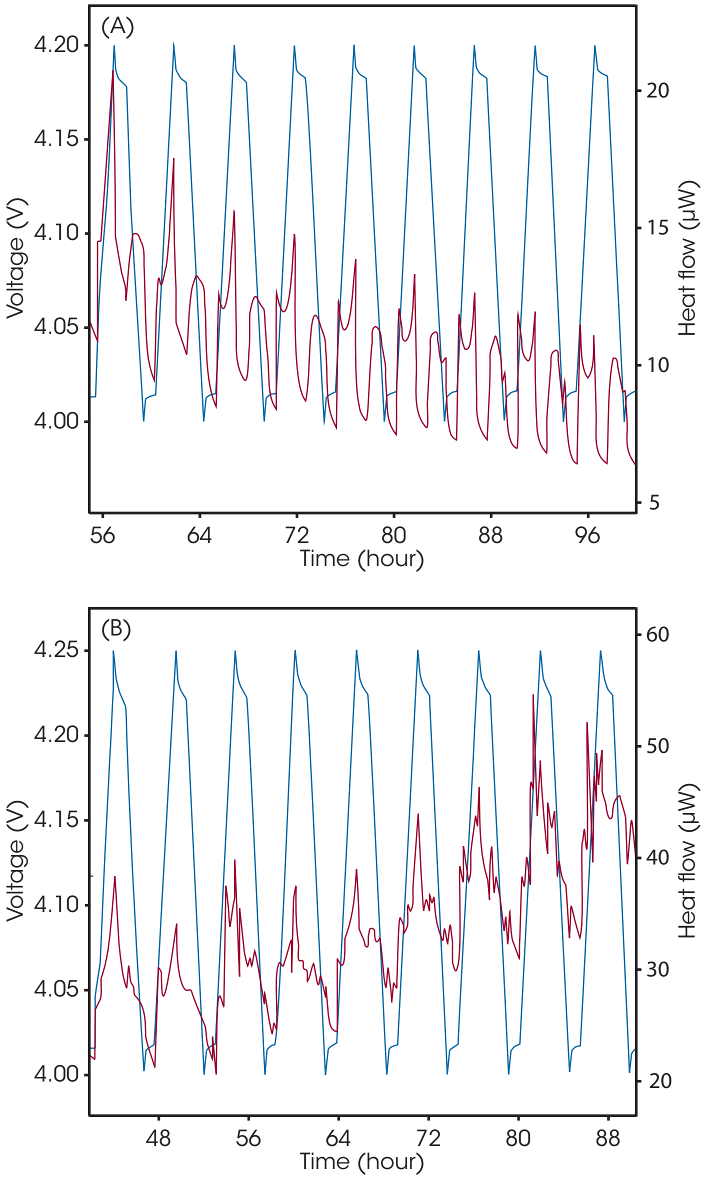

Figure 4. Comparison of thermogram behavior for Cell 1 (A) and Cell 2 (B) during the narrow cycle phase

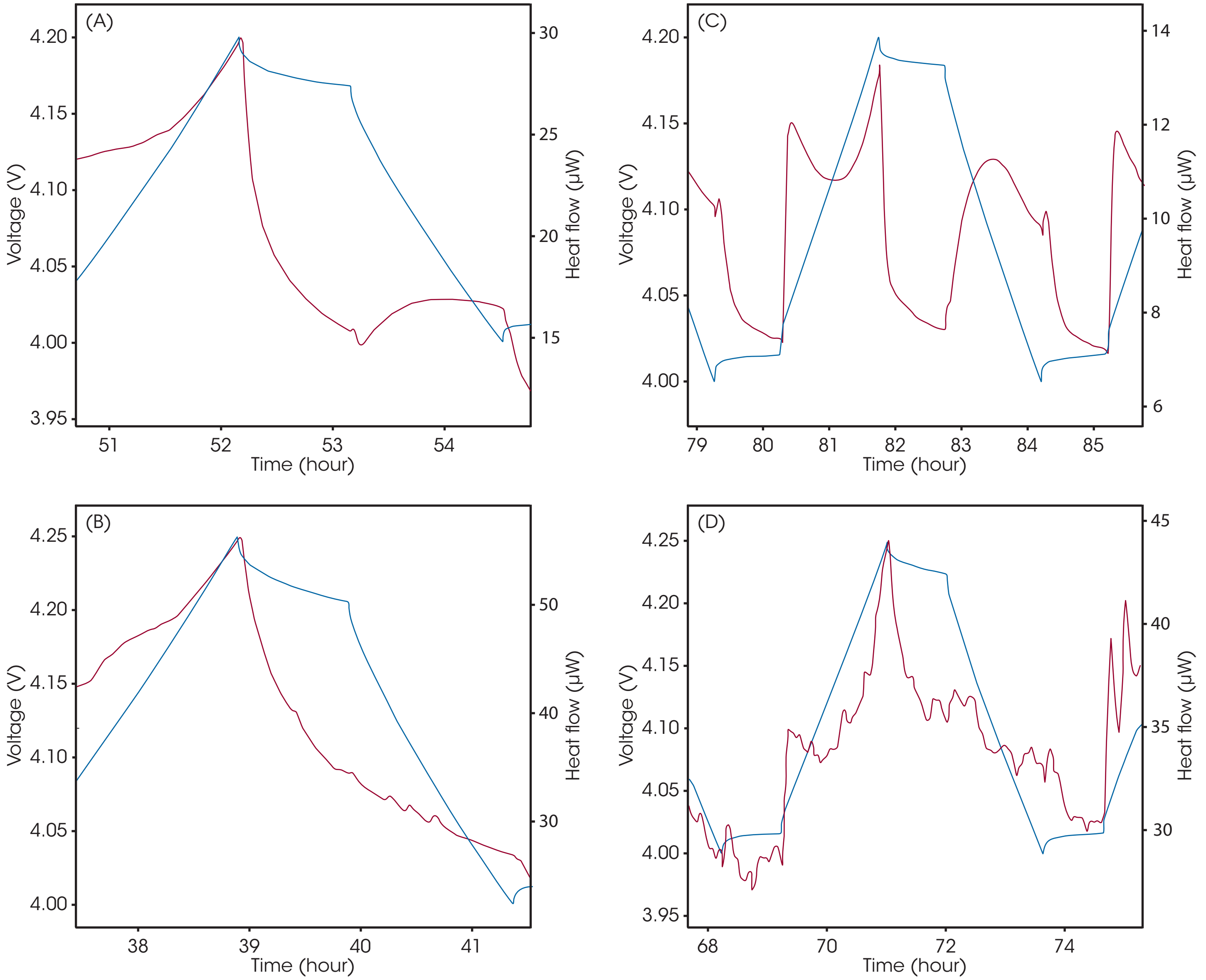

Figure 5. Close examination of the first narrow cycle for (A) Cell 1 and (B) Cell 2 and the seventh narrow cycle of (C) Cell 1 and (D) Cell 2

Figures 5A and 5B show a detailed view of the first narrow cycle. During this cycle, Cell 2 was overcharged to 4.25 V for the first time, and the effects of this overcharge are seen in the thermogram of Figure 5B. One small exotherm is observed during the open circuit rest period, followed by three more during the discharge step. These small exotherms, approximately 1 µW, are well above the short-term noise for the microcalorimeter (~±100 nW) and are not observed in Cell 1 (Figure 5A). If lithium metal is plating on the anode, an exothermic event would be expected in the thermogram as lithium metal reacts with the electrolyte. These small exotherms are likely the earliest occurrence of this process, given the overcharged state and the eventual behavior observed in Figure 3B.

To highlight the difference in thermogram activity between the two cells, Figures 5C and 5D show a closer view of the seventh narrow cycle.

Cell 1 (Figure 5C) experiences smooth changes in the heat flow that repeatedly correlate with the cell voltage and SOC. Cell 2, shown in Figure 5D, has a generally elevated heat flow and the increasing rate of chemical side reactions causes changes to the thermogram between cycles. These reactions continue when the cell is at rest, contributing to the general instability of the chemistry. Figure 5 highlights the importance of calorimetric measurements; the difference between the two cells appears obvious from the thermograms but there are no distortions or other anomalies in the voltage profile that would indicate these cells are undergoing very different processes.

The analysis for the narrow cycle segments of Cell 1 and Cell 2 are shown in Figure 6. Overall, the results suggest an increase in parasitic reactions in the overcharged cell and show no indication of a short circuit in either cell. Figure 6A shows the heat flow contribution of parasitic reactions, calculated using Equation 2. A more detailed description of this method can be found in MC169 [6].

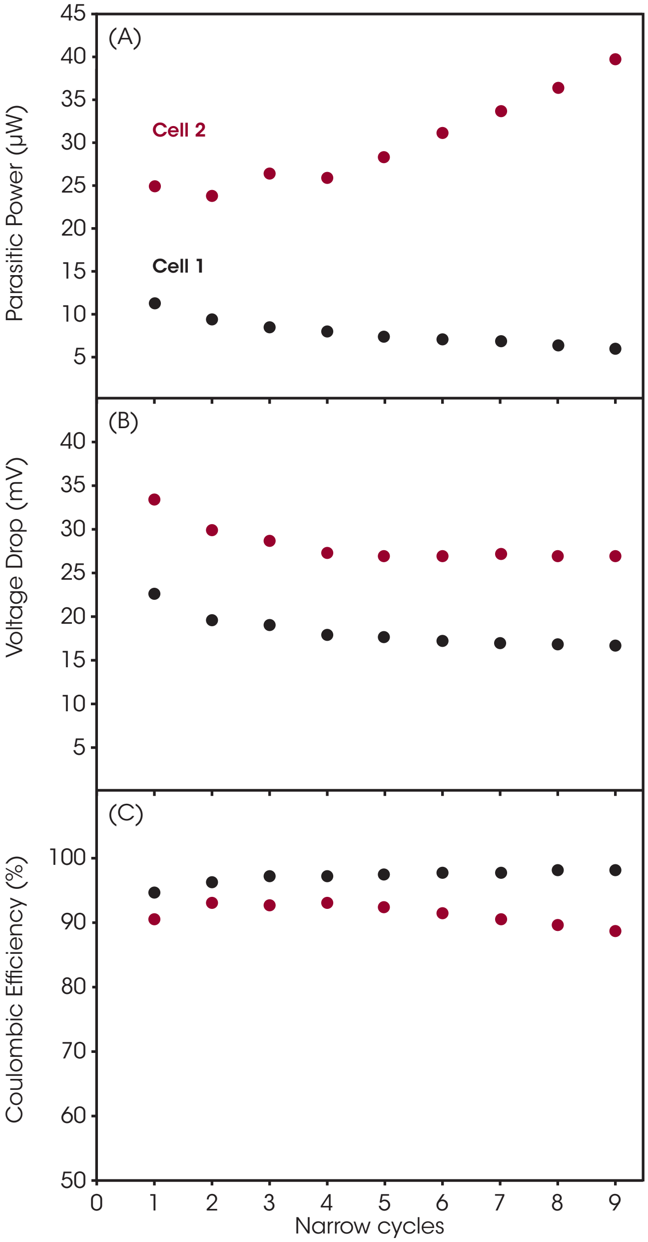

Figure 6. The (A) parasitic heat, (B) voltage drop after the charging step, and (C) coulombic efficiency for Cell 1 (black dots) and Cell 2 (red dots) during the narrow cycle phase

$$Q_{Par} = \left[\int_0^{t_d} \frac{dQ_d}{dt}dt + \int_0^{t_c} \frac{dQ_c}{dt}dt\right] - \left[\int_0^{t_c} I_c V_c dt - \int_0^{t_d} I_d V_d dt\right] \qquad (2)$$

Where:

Q_{Par} is the parasitic heat

Q is the total heat

I is current

V is voltage

subscript "*d*" indicates discharge

subscript "*c*" indicates charging

The rate of parasitic reactions in Cell 1 decreases each cycle, showing a normal rate of passivation for a newly formed cell. Cell 2 shows both a higher magnitude and an increasing rate of parasitic processes per cycle. While a higher rate of parasitic reactions is expected at higher voltages, the increasing trend indicates either a destabilization of the SEI layer or an increasing rate of a different parasitic process, such as lithium metal plating.

Figure 6B shows the overpotential, or voltage drop at 100% state-of-charge (SOC), for both cells. The overpotential is the difference between the voltage when charging and the open circuit voltage, measured near the end of the rest period, as seen in Equation 3.

$$\eta = V_{oc} - V_L \qquad (3)$$

Where:

η is the overpotential

V_{oc} is the open circuit or equilibrium voltage

V_L is the voltage when under electrical load.

This is typically measured as an indication for the SOC-dependent cell resistance, but significant voltage drops also indicate a loss in charge. The difference in overpotential between Cell 1 and 2 is roughly 10 mV. This is a relatively minor difference, and a small degree of variation can be attributed to the difference in upper cell voltages (4.20 V vs 4.25 V). However, the trend between the cycles is the same, and neither cell shows any sign of an internal short circuit or loss of charge. The coulombic efficiency of the two cells is shown in Figure 6C. These results are consistent with Figure 6A, indicating a greater energy loss from side reactions in Cell 2 relative to Cell 1. While the parasitic heat is a more sensitive method to quantify cycle efficiency, the coulombic efficiency is useful for validating the calorimetric measurement. Overall, the data in Figure 6 indicates an increased rate of side reactions occurring in the overcharged cell, but no indication of an internal short circuit.

Comparisons of the three full cycles following the narrow cycle phase are shown in Figure 7A and 7B for Cells 1 and 2, respectively. The exotherms from Li metal reacting with the electrolyte are present, but less of a dominant feature in the full cycle thermogram due to the difference in scale. Cell 1 produces a smooth and repeatable thermogram between cycles, consistent with the narrow phase cycle highlighted in Figure 4A. The heat flow magnitude of Cell 2 is higher and increases significantly with each cycle. In the second full cycle, Cell 2 experiences a series of large step changes in heat flow that increase the baseline heating by a significant margin. These step changes are most likely due to lithium metal dendrites forming internal short circuits.

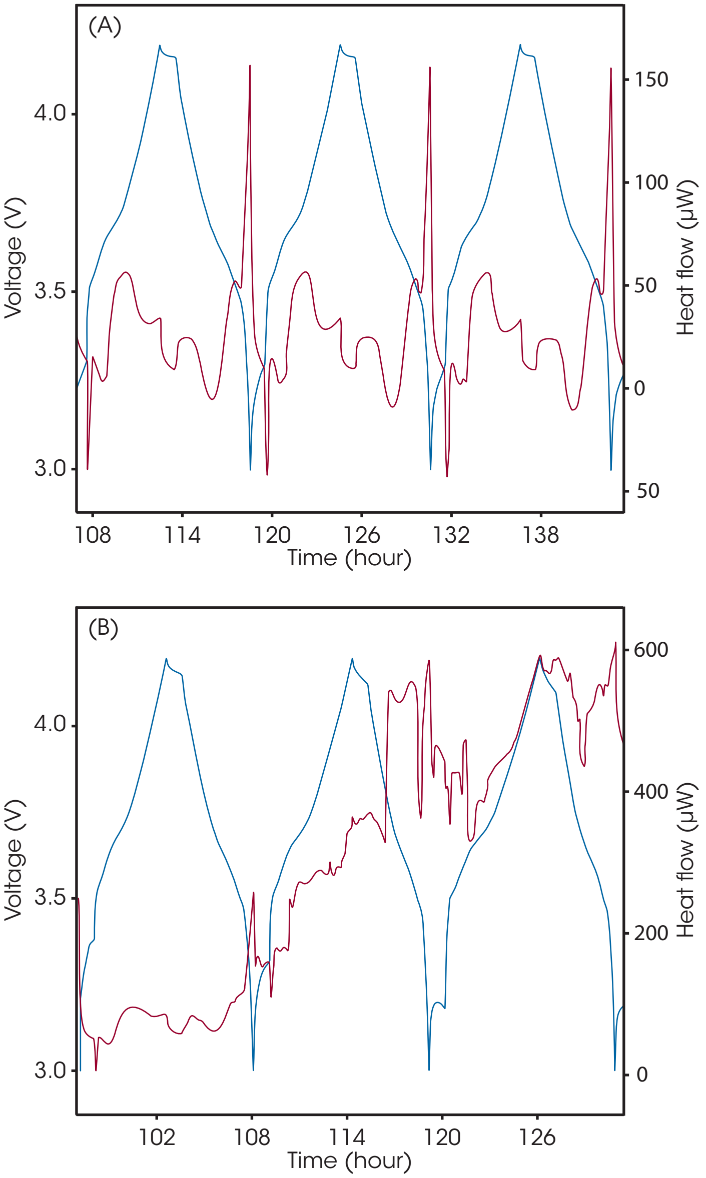

Figure 7. Comparison of full cycle thermogram behavior for (A) Cell 1 and (B) Cell 2

Figure 8 shows the voltage drop at 100% SOC, and coulombic efficiency, and parasitic power for the full cycles shown in Figure 7. The open circuit voltage drops, visible in the second and third cycle of Figure 7, are plotted in Figure 8A. These voltage drops are the result of capacity leakage, or the loss of stored energy. The magnitude and sudden onset in the second full cycle are strong evidence for an internal short. A similar trend is seen in the Coulombic Efficiency, seen in Figure 8B. A slow internal short will increase the charge time, decrease the discharge time, and cause significant drops in coulombic efficiency. Accompanying the increase in total heat flow, the parasitic heat, shown in Figure 8C, also increased significantly in the second and third full cycle. An elevated rate of side reactions are expected in Cell 2, but the magnitude is likely inflated by the higher degree of asymmetry between charge and discharge.

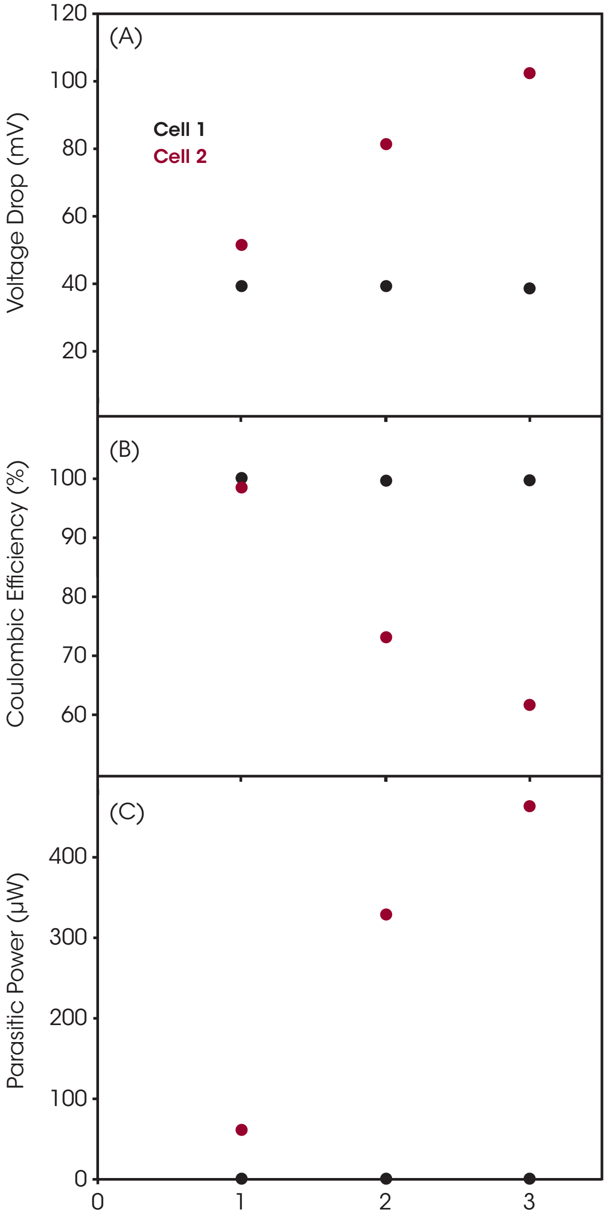

Figure 8. The (A) voltage drop after the charging step, (B) coulombic efficiency and (C) parasitic power for Cell 1 (black dots) and Cell 2 (red dots), during the full cycle phase

From the analysis in Figure 8, the evidence in the electrochemical data is strong for the development of an internal short circuit during the second full cycle of Cell 2. This corresponds the significant increase in heat flow during the same cycle. This is the point in the electrochemical data where evidence for an imminent failure becomes apparent. However, the heat flow data showed significant signs of instability roughly 3 days prior. The first time Cell 2 was overcharged, small exotherms were observed in the heat flow, corresponding to the reaction between lithium metal and the electrolyte [12]. From this initial onset, the intensity of these side reactions grew until the short circuit occurred and the rapid self-heating began.

CONCLUSIONS

Stabilization of the lithium metal-electrolyte interface and the suppression of dendrite formation is an ongoing challenge for battery researchers. Lithium dendrite propagation reduces the energy storage efficiency, causes cell failure through internal short circuits, and in some cases leads to a full thermal runaway reaction.

High sensitivity microcalorimetry using the TA Instruments Battery Cycler Microcalorimeter Solution will allow researchers to detect the early onset of lithium dendrite formation and to quantify the efficacy of their dendrite suppression strategies. Electrochemical microcalorimetry will prove to be an essential tool in both the fundamental study of failure mechanisms and in discovering methods to ultimately prevent cell failure.

REFERENCES

1. "TA467: Safety Evaluation of Lithium-ion Battery Cathode and Anode Materials Using Differential Scanning Calorimetry." [Online] Available: https://www.tainstruments.com/pdf/literature/TA467.pdf.
2. "TA470: Thermogravimetric Analysis of Powdered Graphite for Lithium-ion Batteries." [Online] Available: https://www.tainstruments.com/pdf/literature/TA4470.pdf.
3. "TA480: Thermal Evaluation of LFP Li-Ion Battery Cathodes using Simultaneous DSC-TGA (SDT)." [Online] Available: https://www.tainstruments.com/pdf/literature/TA4480.pdf.
4. K. Liu, Y. Liu, D. Lin, A. Pei, Y. Cui. Materials for lithium-ion battery safety. *Sci. Adv*., **2018**, *4*, eaas9820.
5. "MC162: The Impact of Electrolyte Additives in Lithium-ion Batteries Determined Using Isothermal Microcalorimetry." [Online] Available: https://www.tainstruments.com/pdf/literature/MC162.pdf.
6. "MC169: Determination of Parasitic Power in Lithium-ion Batteries using the Battery Cycler Microcalorimeter Solution." [Online] Available: https://www.tainstruments.com/pdf/literature/MC169.pdf.
7. L.E. Downie, L.J. Krouse, J.C. Burns, L.D. Jensen, V.L. Chevrier, J.R. Dahn. In Situ Detection of Lithium Plating on Graphite Electrodes by Electrochemical Calorimetry. *Journal of The Electrochemical Society,* **2013**, *160 (4),* A588-A594.
8. J.C. Burns, D.A. Stevens, J.R. Dahn. In-Situ Detection of Lithium Plating Using High Precision Coulometry. *Journal of The Electrochemical Society*, **2015**, *162 (6)*, A959-A-964.
9. H. Xu, C. Han, W. Li, H. Li, X. Qiu. Quantification of lithium dendrite and solid electrolyte interphase (SEI) in lithium-ion batteries. *Journal of Power Sources,* **2022**, *529,* 231219.
10. J. Asenbauer, T. Eisenmann, M. Kuenzel, A. Kazzazi, Z. Chen, D. Bresser. The success story of graphite as a lithium-ion anode material – fundamentals, remaining challenges, and recent developments including silicon (oxide) composites. *Sustainable Energy Fuels,* **2020**, *4*, 5387-5416.
11. Q. Zhao, Y. Deng, N. Utomo, J. Zheng, P. Biswal, J. Yin, L. Archer. On the crystallography and reversibility of lithium electrodeposits at ultrahigh capacity. *Nature Communications,* **2021**, *12*, 6034.
12. K. Kanamura, H. Takezawa, S. Shiraishi, Z. Takehara. Chemical Reaction of Lithium Surface during Immersion in LiClO4 or LiPF6 / DEC Electrolyte. *Journal of The Electrochemical Society,* **1997**, *144*, 1900.

ACKNOWLEDGMENTS

For more information or to request a product quote, please visit www.tainstruments.com to locate your local sales office information.

This paper was written by Jeremy May, PhD.